inorganics

MDPI

Article

Heteroleptic and Homoleptic Iron(III) Spin-Crossover Complexes; Effects of Ligand Substituents and Intermolecular Interactions between Co-Cation/Anion and the Complex

Wasinee Phonsri, Luke C. Darveniza, Stuart R. Batten and Keith S. Murray *

School of Chemistry, Building 23, 17 Rainforest Walk, Monash University, Clayton, VIC 3800, Australia; wasinee.phonsri@monash.edu (W.P.); lcdar2@student.monash.edu (L.C.D.); stuart.batten@monash.edu (S.R.B.)

* Correspondence: keith.murray@monash.edu; Tel.: +61-399-054-512; Fax: +61-399-054-597

Received: 19 June 2017; Accepted: 28 July 2017; Published: 1 August 2017

Abstract: The structural and magnetic properties of a range of new iron(III) bis-tridentate Schiff base complexes are described with emphasis on how intermolecular structural interactions influence spin states and spin crossover (SCO) in these d^5 materials. Three pairs of complexes were investigated. The first pair are the neutral, heteroleptic complexes [Fe(3-OMe-SalEen)(thsa)] **1** and [Fe(3-MeOSalEen)(3-EtOthsa)] **2**, where 3-R-HSalEen = (*E*)-2-(((2-(ethylamino)ethyl)imino)methyl)-6-R-phenol and 3-R-H_2thsa = thiosemicarbazone-3-R-salicylaldimine. They display spin transitions above room temperature. However, **2** shows incomplete and gradual change, while SCO in **1** is complete and more abrupt. Lower cooperativity in **2** is ascribed to the lack of π–π interactions, compared to **1**. The second pair, cationic species [Fe(3-EtOSalEen)$_2$]NO_3 **3** and [Fe(3-EtOSalEen)$_2$]Cl **4** differ only in the counter-anion. They show partial SCO above room temperature with **3** displaying a sharp transition at 343 K. Weak hydrogen bonds from cation to Cl^- probably lead to weaker cooperativity in **4**. The last pair, CsH_2O[Fe(3-MeO-thsa)$_2$] **5** and Cs(H_2O)$_2$[Fe(5-NO_2-thsa)$_2$] **6**, are anionic homoleptic chelates that have different substituents on the salicylaldiminate rings of $thsa^{2-}$. The Cs cations bond to O atoms of water and the ligands, in unusual ways thus forming attractive 1D and 3D networks in **5** and **6**, respectively, and **5** remains HS (high spin) at all temperatures while **6** remains LS (low spin). Comparisons are made to other literature examples of Cs salts of [Fe(5-R-thsa)$_2$]$^-$ (R = H and Br).

Keywords: iron(III) complexes; spin crossover; heteroleptic; homoleptic; magnetism; structure; intermolecular interactions; cation–anion interactions

1. Introduction

In recent reviews and monographs on spin-crossover (SCO) materials [1–3], there is a dearth of examples of heteroleptic iron(III) complexes, apart from those of type [Fe(O_2N_2-tetradentate)(L)$_2$]$^+$ where L = pyridine, imidazole etc.; tetradentate = Schiff base [4]. We recently described the first example of an heteroleptic iron(III) spin-crossover complex [Fe(3-OMe-SalEen)(thsa)] **1** containing two *mer*-tridentate Schiff base ligands where 3-OMe-HSalEen = (*E*)-2-(((2-(ethylamino)ethyl)imino) methyl)-6-methoxyphenol and H_2thsa = thiosemicarbazone-salicylaldimine [5]. The donor set in **1** was N_3O_2S. Notably, the complex showed a gradual, complete spin transition above room temperature at 344 K, with enhanced spin-crossover properties compared to homoleptic cationic [Fe(3-OMe-SalEen)$_2$]$^+$ and anionic [Fe(thsa)$_2$]$^-$ analogues. π–π intermolecular interactions between each ligand type were the key reasons for the high $T_{1/2}$ value.

Here, we have extended this work by making reasonably systematic changes to both the tridentate ligands particularly by changing the substituent groups on the salicylaldehyde rings (Scheme 1). We

describe the neutral, heteroleptic complex [Fe(3-MeO-SalEen)(5-NO_2thsa)] **2** and make comparisons to the thsa parent **1** [5]. A pair of cationic homoleptic complexes [Fe(3-EtOSalEen)$_2$]NO_3 **3** and [Fe(3-EtOSalEen)$_2$]Cl **4** are explored to identify any anion effects. In a similar manner, a pair of anionic complexes, CsH_2O[Fe(3-MeOthsa)$_2$] **5** and Cs(H_2O)$_2$[Fe(5-NO_2-thsa)$_2$] **6**, are described that allow us to probe how both ligand substituent and cation–anion effects influence spin states and SCO. Crystallography is used extensively to probe intermolecular interactions in these new materials.

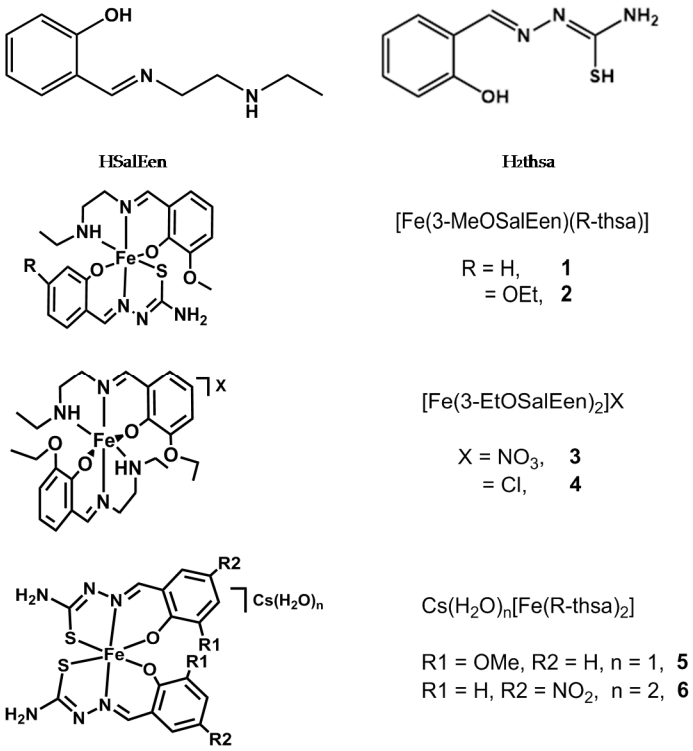

Scheme 1. Molecular structures of HSalEen and H_2thsa ligands together with Fe(III) compounds **1**–**6**. Note that the actual coordination of the Fe(III) compounds will be discussed *vide infra*, the pictures shown here clarify the molecular components only.

2. Results and Discussion

2.1. Preparation of Iron(III) Complexes

The complexes were all formed using layered diffusion techniques. Different combinations of solvents in a reaction depend on the solubility of reactants in each reaction and the layers were constructed according to the density of the solvents. The heteroleptic compound, [Fe(3-MeOSalEen)(3-EtOthsa)] **2**, was formed using an aqueous layer of the 3-EtO-H_2thsa ligand with CsOH in H_2O at the bottom, and a layer of $FeCl_3$ in *n*-butanol was in the middle. Then a layer of another ligand, 3-MeO-HSalEen ligand with triethylamine, in methanol, was on the top. Notably, the solubility of the R-H_2thsa ligands is very poor in water but it can be improved by adding a base to the mixture. The 3-EtOSalEen homoleptic complexes, [Fe(3-EtOSalEen)$_2$]NO_3 **3** and [Fe(3-EtOSalEen)$_2$]Cl **4**, were formed using a layer of ligand in dichloromethane. The bulk sample of **3** required solvated MeOH and water to fit the micro-analytical data. The substituted thsa homoleptic complexes, CsH_2O[Fe(3-MeOthsa)$_2$] **5** and Cs(H_2O)$_2$[Fe(5-NO_2-thsa)$_2$] **6**, were formed using an aqueous layer of ligand and CsOH with a layer of Fe(III) salts, in methanol, on the top. Phase purity of samples used for magnetic study was confirmed by comparison of powder X-ray diffractograms (PXRD) to simulated diffractograms (see Supplementary Figure S1). The PXRD for **6**(**bulk**) fitted well to the crystallographic refinement model (see Sections 2.5 and 3.1); however, the closest fit for the microanalytical data was a

formula $Cs(H_2O)_2[Fe(5\text{-}NO_2\text{-}thsa)_2]\cdot CsOH$ (i.e., **6**·CsOH), suggesting the presence of some amorphous CsOH contaminant in the sample. Thus, as seen above, we have labelled the bulk sample **6**(**bulk**) and the crystals **6**.

2.2. Magnetism

The variable-temperature magnetic susceptibility data for the complexes were obtained within the 5–400 K range without any protective coating applied to the sample. All the experiments were conducted under a DC field of 0.5 T and at a heating/cooling rate of 10 $K\cdot min^{-1}$ in the settle mode, apart from compound **1** that was examined under various sweep rates with the results being reported previously [5]. For compounds **2**–**4**, the plots in Figure 1 all show incomplete SCO up to 360 K. At low temperature, the magnetic susceptibilities are about 0.4–0.5 $cm^3\cdot mol^{-1}\cdot K$, indicative of the compounds being in the LS (low spin) state. Upon warming, the spin transitions begin to take place at around 250 K (for **2**) and 340 K (for **3** and **4**), and show 48%, 36% and 16% degree of spin crossover up to 360 K, respectively. The $\chi_M T$ values of the compounds tend to keep increasing at higher temperature but, unfortunately, do not reach fully the HS (high spin) value at 400 K. It is noted that compound **3** exhibits an abrupt, reproducible spin transition with a 3 K hysteresis width ($T\uparrow$ = 343 K), while **2** and **4** show gradual changes. The small change in $\chi_M T$ at the abrupt transition in **3** suggests that only some fraction of the material is showing this transition. On the other hand, compounds **5** and **6**(**bulk**) show invariant HS and LS behaviour, respectively (Figure S2). All the magnetic results agree well with the single-crystal structure data of **1**–**6**.

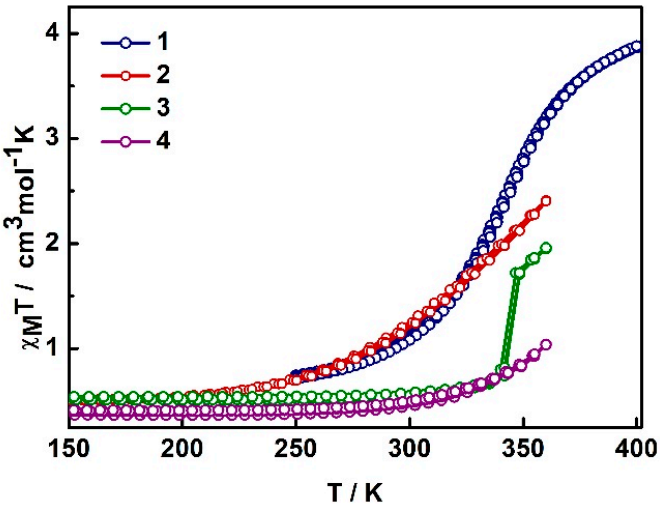

Figure 1. Variable-temperature magnetic susceptibility ($\chi_M T$) measurements for compounds **1**–**4**.

2.3. Structural Study of Heteroleptic Fe(III) Compounds **1** and **2**

The crystal structures of [Fe(3-MeOSalEen)(thsa)] **1** and [Fe(3-MeOSalEen)(3-EtOthsa)] **2** have been examined at 100 K. The data revealed that the structure of **2** crystallizes in the monoclinic, $P2_1/c$ space group (Table 1). Details of the crystal structure of **1** have been presented [5] and are given in Tables 1 and 2. In the asymmetric unit, for both **1** and **2**, there is a neutral molecule of the Fe(III) compound where the metal centres coordinate to N_3O_2S donors belonging to 3-MeOSalEen$^-$ and R-thsa^{2-} ligands where R = H **1**, 3-EtO **2** (Figure S3). For compound **2**, the Fe–L bond lengths and the octahedral distortion parameters are shown in Table 2. Fe–O, Fe–N and Fe–S bond lengths are 1.88–1.93, 1.91–1.94 (for 3° amine) 2.05 (for 2° amine), and 2.25 Å, respectively. These bond lengths agree with the low values of the octahedral distortion parameters [6,7] (Σ = 51° and Θ = 98°) and all are indicative of the low spin state (LS) of the Fe(III) centre at 100 K.

Table 1. Crystallographic data and structure refinement for **1–6**.

Complex	1 [5]	2	3	4	5	6
Temp.	100 K	100 K	100 K	100 K	123 K	123 K
Molecular weight/g·mol^{-1}	470.35	514.40	588.45	561.90	653.28	701.25
Crystal system	Triclinic	Monoclinic	Triclinic	Triclinic	Orthorhombic	Tetragonal
Space group	$P\bar{1}$	$P2_1/c$	$P\bar{1}$	$P\bar{1}$	*Pnna*	$P\bar{4}n2$
a/Å	8.3940 (17)	14.122 (3)	9.646 (2)	9.698 (2)	19.0649 (7)	20.6177 (3)
b/Å	9.3500 (19)	13.889 (3)	10.632 (2)	10.633 (2)	9.1084 (4)	20.6177 (3)
c/Å	13.675 (3)	13.470 (3)	14.242 (3)	13.515 (3)	13.1902 (5)	11.7467 (3)
α/°	82.26 (3)	90	100.25 (3)	96.15 (3)	90	90
β/°	73.44 (3)	118.40 (3)	105.21 (3)	103.05 (3)	90	90
γ/°	82.14 (3)	90	102.93 (3)	103.49 (3)	90	90
Cell volume/Å^3	1013.9 (4)	2324.1 (10)	1329.5 (5)	1301.3 (4)	2290.5 (2)	4993.4 (2)
Z	2	4	2	2	4	8
Absorption coefficient/mm^{-1}	0.880	0.778	0.622	0.722	2.451	2.266
Reflections collected	27,497	23,856	24,637	21,725	42,177	188,772
Independent Reflections, R_{int}	5929, 0.0501	6297, 0.0369	6224, 0.0792	5703, 0.1664	3544, 0.0582	10084, 0.0651
Max., min. transmission	0.9913, 0.9741	0.9923, 0.977	0.9969, 0.9695	0.9964, 0.9857	0.9301, 0.7493	0.7727, 0.6600
Restraints/parameters	1/277	0/301	0/364	0/329	0/156	12/331
Final R indices [$I > 2\sigma(I)$]: R_1, wR_2	0.0401, 0.1123	0.0408, 0.1118	0.0419, 0.1111	0.0573, 0.1518	0.0298, 0.0648	0.0747, 0.2314
CCDC No.	1420398	1552518	1552515	1552514	1552517	1552516

Data for **2–6**, this work. CCDC number from Cambridge Crystallographic Data Base deposition number.

Table 2. Selected bond lengths and octahedral distortion parameters for **1–6**.

Complex	1 [5]	2		3	4		5		6
Temp.	100 K	100 K		100 K	100 K		123 K		123 K
Fe1–O1/Å	1.8875 (14)	1.882 (1)	Fe1–O2/Å	1.877 (1)	1.874 (2)	Fe1–O1/Å	1.987 (2)	Fe1–O1/Å	1.917 (6)
Fe1–O3/Å	1.8937 (13)	1.9315 (1)	Fe1–O4/Å	1.889 (2)	1.895 (2)	Fe1–O1 ^{iii}/Å	1.987 (2)	Fe1–O2/Å	1.922 (5)
Fe1–N1/Å	2.2590 (8)	2.050 (2)	Fe1–N1/Å	1.926 (2)	1.923 (3)	Fe1–N1/Å	2.179 (2)	Fe1–N1/Å	1.931 (6)
Fe1–N2/Å	2.0588 (17)	1.915 (2)	Fe1–N2/Å	2.037 (2)	2.041 (3)	Fe1–N1 ^{iii}/Å	2.179 (2)	Fe1–N4/Å	1.911 (6)
Fe1–N3/Å	1.9198 (14)	1.942 (2)	Fe1–N3/Å	2.060 (2)	2.046 (3)	Fe1–S1/Å	2.416 (1)	Fe1–S1/Å	2.214 (2)
Fe1–S1/Å	1.9424 (14)	2.248 (1)	Fe1–N4/Å	1.923 (2)	1.922 (3)	Fe1–S1 ^{iii}/Å	2.416 (1)	Fe1–S2/Å	2.237 (2)
Σ/°	44	51	Σ/°	47	48	Σ/°	129	Σ/°	39
Θ/°	80	98	Θ/°	70	72	Θ/°	404	Θ/°	67

Symmetry codes: (iii) x, $-y+1/2$, $-z+1/2$. Data for **2–6**, this work.

Although both **1** and **2** are in the LS state at low temperatures, compound **2**, with its extra ethoxy group substituted on the 3 position of the thsa^{2-} ligand, has a higher degree of distortion around the metal centre. It is obvious that the octahedral distortion parameters are higher in the case of **2** than in **1**, especially in the case of the Θ value that differs by 18°. Accordingly, the angle between the planes of thsa^{2-} ligand in **2** are larger than that angle is in **1** by about 10° (Table S1). On the other hand, for the 3-OMeSalEen^{-} ligand, the angle between the ligand planes in **1** and **2** shows smaller differences by about 3° (Figure S4). The superimposition of the Fe(III) molecules of **1** and **2** is illustrated in Figure 2. Unexpectedly, the orientation of the ethane moiety in the 3-MeOSalEen^{-} ligand for **1** and **2** bends out of the plane in the opposite direction. Therefore, the 3-EtO substituent on the thsa^{2-} ligand affects the arrangement of both thsa^{2-} itself as well as the 3-MeOSalEen^{-} ligand.

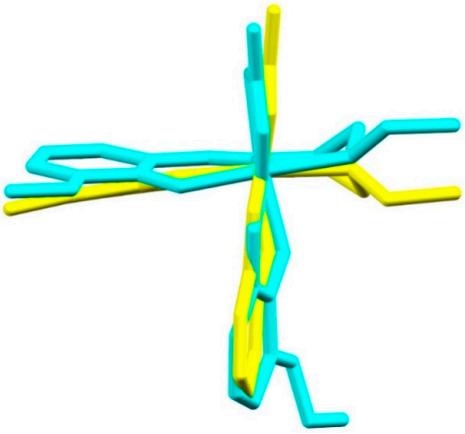

Figure 2. Superimposition of the Fe(III) molecules of 1 (yellow) and 2 (cyan) in a "wireframe" model.

Crystal packing in solid-state spin-crossover complexes is important in regard to explaining cooperativity and other spin-crossover nuances. According to the packing of **1** and **2**, the 1D chain motif along the *b* axis is similar and involves interactions via C–H···S and N–H···N. This is the only one direction that the 3-EtO group in **2** does not affect the crystal packing and shows similar packing as **1** (Figure 3). As the 3-EtO substituent on the thsa^{2-} ligand occupies space above the 3-OMeSalEen^{-} ligand (Figure S3b), it prevents another ligand from coming close and forming π–π interactions. Therefore, there are no π–π interactions present in **2**. In **1**, however, strong π–π interactions were claimed to be a key reason for the high $T_{1/2}$ value observed [5]. The Fe(III) moieties in **2** form a chain through C–H···C/π interactions instead of connecting through two sets of strong π–π interactions as was found in **1** (Figure S5). Likewise, in the last dimension along the *a* axis, a continuous chain from two sets of π–π interactions links a plane of **1** into a high dimensional structure with a high degree of packing order (Figure S5a). Whilst there are weak C–H···C/π interactions found in the case of **2**, it is suggested that adding an extra 3-EtO on the thsa^{2-} ligand in **2** reduces the structural order in the structure, not only in the isolated Fe(III) molecule, but also in the overall packing of the structure (Figure S6b). Consequently, the molecules are unable to form π–π interactions. In summary, this is suggested to lead to a decrease in the cooperativity in **2** and result in the incomplete SCO (see above).

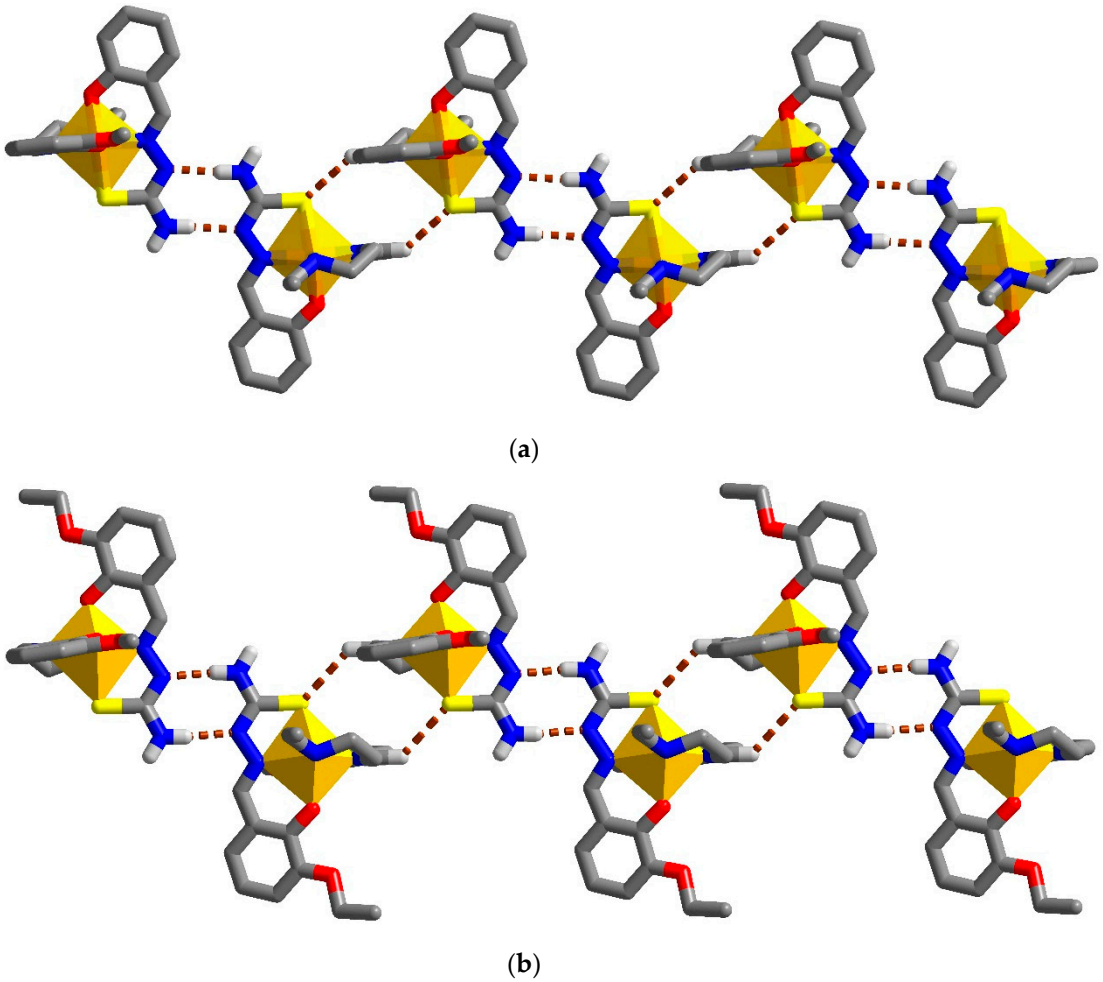

Figure 3. C–H···S and N–H···N interactions that show similarly connecting Fe(III) molecules in (**a**) **1** and (**b**) **2**. Colour coding: O, red; N, blue; S, yellow; C, grey; H, white; yellow octahedra show coordination environment around Fe.

2.4. Structural Study of Homoleptic Cationic Fe(III) Compounds **3** *and* **4**

The crystal structures of $[Fe(3\text{-}EtOSalEen)_2]NO_3$ **3** and $[Fe(3\text{-}EtOSalEen)_2]Cl$ **4** have also been investigated at 100 K. The data revealed that both structures are crystallized in the triclinic, $P\bar{1}$ space group (Table 1). With a slightly bigger anion, the cell volume of **3** is rather larger than that of **4** by about 28 Å^3. It is noted that the *c* parameters of the unit cell in **3** are significantly larger than that in **4** compared to other dimensions. This is because the NO_3^- and Cl^- anions occupy space between the Fe(III) sheets along the *c* axis (Figure S7). The size of the anions then influences the size of the unit cell along the *c* axis more than the other axes. For the asymmetric unit of **3** and **4**, a cationic molecule of $[Fe(3\text{-}EtOSalEen)_2]^+$ co-exists with the counter anions (Figure 4). A Fe(III) centre coordinates to the N_4O_2 donors from two of 3-EtOSalEen$^-$ ligands disposed in the meridional fashion. The Fe–L bond lengths and octahedral distortion parameters shown in Table 2 are in the same ranges as in **1** and **2**, which again suggests that the LS state exists at the Fe(III) centres of **3** and **4** at low temperature.

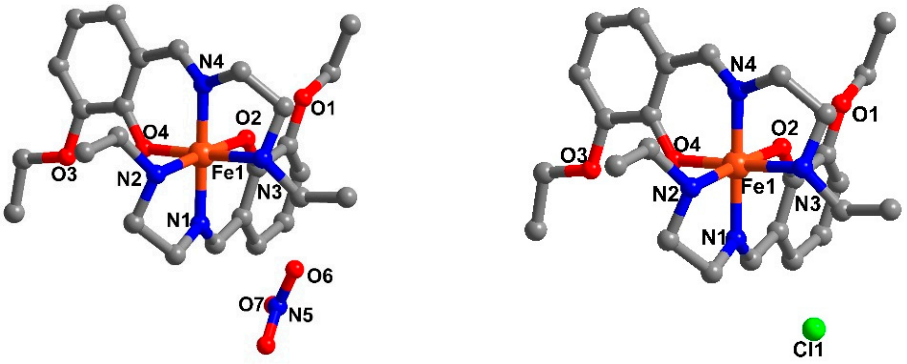

(**a**) (**b**)

Figure 4. Representation of the asymmetric unit components for (**a**) **3** and (**b**) **4**. Hydrogen atoms are omitted for clarity.

Compounds **3** and **4** are isostructural. Both the Fe (III) moieties and the counter anions are located on the same position (Figure S8). Along the *a* axis, $[Fe(3\text{-}EtOSalEen)_2]^+$ interacts with the neighbouring molecules mainly through the parallel fourfold aryl embrace (P4AE) [8] and C–H···π interactions (Figure 5). All details of the interactions are shown in Tables S3 and S4. It is noted that these P4AE interactions do not show any relation to the magnetic behaviour of the compounds, as can be seen in Table S5. This is in agreement with our previous work that suggested a strong correlation between the π–π interactions (not P4AE) and SCO properties in this system [5]. In other dimension, the molecules connect through weak hydrogen bonds mainly involving the anion groups (Figure S9).

As mentioned, **3** and **4** are isostructural and only the anions are different between these two compounds. It is interesting to note that **3** shows an abrupt 50% SCO with a small thermal hysteresis width, while **4** exhibits a gradual incomplete spin change (see magnetism section). To try to understand these differences, the crystal structures of **3** and **4** are thoroughly investigated particularly in regard to intermolecular interactions involving the anions. It is found that some of the interactions relating to NO_3^- in **3**,where there are linking Fe(III) moieties forming an extended structure, utilise moderate hydrogen bonds, while, those for Cl^- in **4** are all of the weak hydrogen bond type [9] (Table S4). Thus, it is suggested to give rise to poorer cooperativity in **4** and lead to a gradual incomplete SCO appearing in this compound. It is possible that electronic effects provided by NO_3^- and Cl^- are partly responsible for the magnetic properties of the compounds but theoretical calculation would be required to prove this.

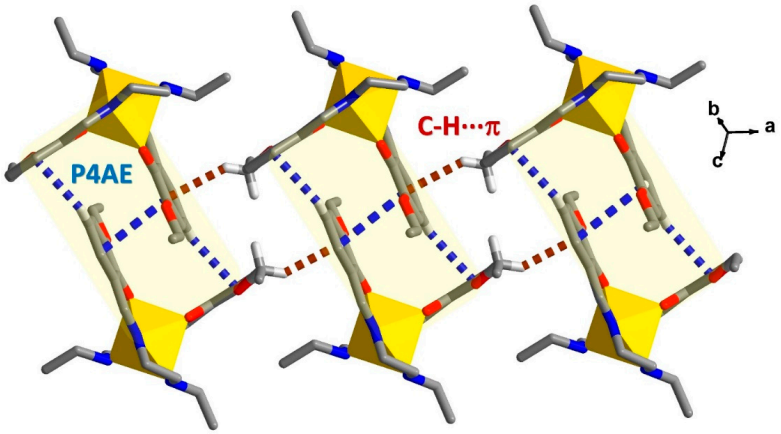

Figure 5. The 1D chain packing motif in **3** and **4** involving P4AE [8] and C–H···π interactions. Colour coding: O, red; N, blue; C, grey; H, white; yellow octahedra show coordination environment around Fe.

2.5. Structural Study of Homoleptic Anionic Fe(III) Compounds **5** and **6**

Six-coordinate Fe(III) compounds containing two substituted di-anionic ligands, R-H_2thsa with Cs^+ counter cations, viz. CsH_2O[Fe(3-MeOthsa)$_2$] **5** and Cs(H_2O)$_2$ [Fe(5-NO_2-thsa)$_2$] **6**, have been studied. Single-crystal data for the compounds are given in Table 1. The data show that the structure of **5** is crystallized in the orthorhombic, *Pnna* space group, while the crystal structure of **6** is in the tetragonal, $P\bar{4}n2$ system. The contents of the asymmetric units of the compounds are illustrated in Figure 6 and show a half molecule of [Fe(3-MeOthsa)] with a half occupancy of Cs cation in that of **5**, while for **6** a molecule of [Fe(5-NO_2-thsa)$_2$]$^-$ exists together with two Cs cations with a half occupancy at each site of Cs^+. Selected Fe–L and Cs–O bond lengths are shown in Table S2 and Table S6. Notably, Cs cations in both **5** and **6** form bonds with O atoms of the ligands and water molecules, which is different from previous reports of Fe(III)-thsa with Cs cations that also showed Cs–N and Cs–S bonds with R-thsa^{2-} ligands, where R = H [10] and Br [11].

The Fe(III) centres in **5** and **6** possess an octahedral geometry coordinating via $N_2O_2S_2$ donors in a meridional fashion provided by two R-thsa$_2^{2-}$ ligands. According to the Fe–L bond lengths in Table 2, the data for **6** are similar to the Fe–L bond lengths of Fe(III) to 3-EtOthsa^{2-} ligand in **2**, which also suggests the LS state at the metal centre. In the case of **5**, the Fe–L lengths are larger than those in **6** by about 0.07, 025 and 0.2 Å for Fe–O, Fe–N and Fe–S, respectively. Moreover, the high values of octahedral distortion parameters, particularly the Θ ca. 400°, indicate the high degree of distortions around the Fe(III) centre. All the data are indicative to the HS state being populated in **5** at low temperature.

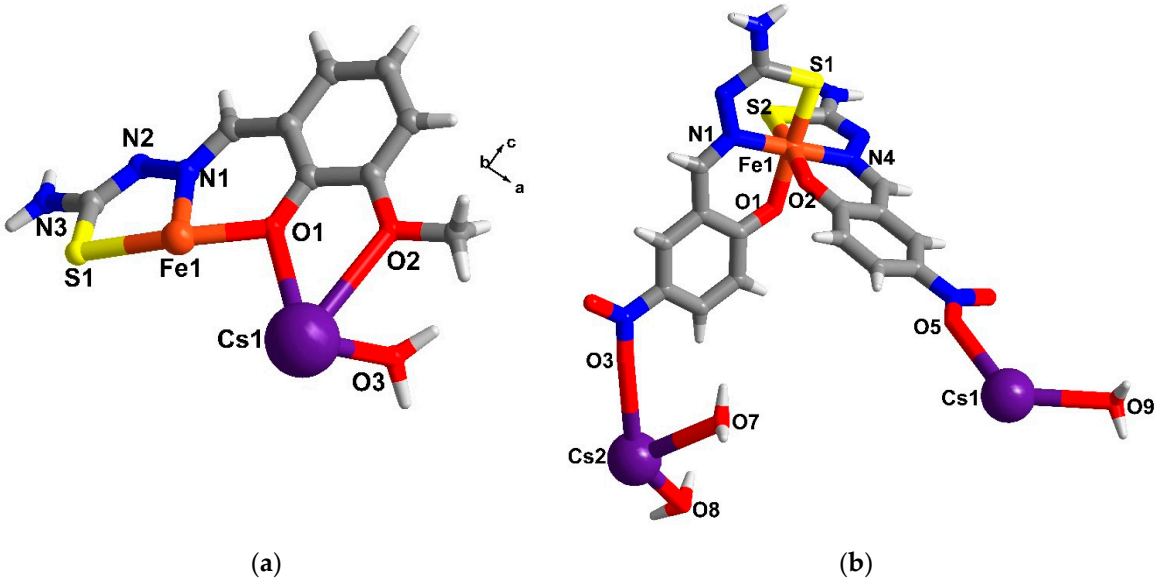

Figure 6. Representation of the asymmetric unit of (**a**) **5** and (**b**) **6**. Notably, some atoms contain 0.5 occupancy in the asymmetric unit i.e., Fe1, Cs1 and O3 in **5**, and Cs1, Cs2, O8 and O9 in **6**.

In an extended structure of **5**, two Cs^+ atoms form coordination bonds with [Fe(3-MeOthsa)$_2$]$^-$ through mono-dentate O2, and μ_4-O1 that acts as a bridging atom between two Cs cations (Figure 7a). This building unit links to the other neighbouring units through Cs–O3(H_2O) and forms a polymer chain along the *b* axis (Figure 7b). In higher dimension, N–H···π/S interactions play a role in connecting polymer chains into a pseudo 3D structure (Figure S11). As mentioned, the distortion parameters (Σ and Θ) for **5** are surprisingly high compared to other HS structures of Fe(III) compounds [3]. According to Figure 7a, one Cs^+ bonds to two O1 from two different 3MeO-thsa^{2-} ligands, and one O1 atom also bridges two Cs atoms. As O1 is a direct donor to the Fe(III) centre, these Cs–O1 coordination bonds thus give rise to an unexpectedly high degree of the distortion surrounding the Fe(III) centre

(Figure S10). Moreover, Cs–O1 bonds are suggested to reduce the electron density around the Fe(III) ion. Consequently, a small energy gap (Δ_{oct}) results in the invariant HS behaviour being observed in **5** (see magnetism section).

In the case of the crystal packing in **6**, each Cs atom connects to the same Cs type in different fashions as shown in Figure 8, to give Cs_2 (for Cs1) and Cs_4 (for Cs2, ignoring the partial occupancy (see Section 3.1)) clusters. The $[Fe(5\text{-}NO_2\text{-}thsa)_2]^+$ cation in turn coordinates to one Cs_4 and one Cs_2 cluster through Cs–O(NO_2-$thsa^{2-}$) interactions (Figure S12b), and a second Cs_2 cluster through interactions between Cs1 and one of the phenol oxygens (O1). All the Cs–O bond lengths in **5** and **6** are shown in Table S6. For Cs1, Cs1–O bonds are formed with four different Fe(III) molecules (Figure 8a), yielding a chain along the *c* axis. The Cs1 chain bridges to the adjacent Cs1 chain via μ_2-O9(H_2O), giving rise to a double polymeric chain of Cs1 and $[Fe(5\text{-}NO_2\text{-}thsa)_2]$ (Figure 8c). On the other hand, Cs2 atoms form a four-member cluster with two μ_2-O(H_2O) bridges (Figure 8b). Overall, each dimer of Cs1 atoms is thus connected to eight Fe(III) complexes (four through each Cs1 atom), while the tetramer of Cs2 atoms is connected to four Fe(III) complexes (one per Cs2 atom). In turn, the Fe complex is coordinated to three Cs clusters, to give a complicated 3,4,8-c 3D net with $(4.8^2)_4(8^6)(4^{12}.8^8.10^8)$ topology (Figure 8d).

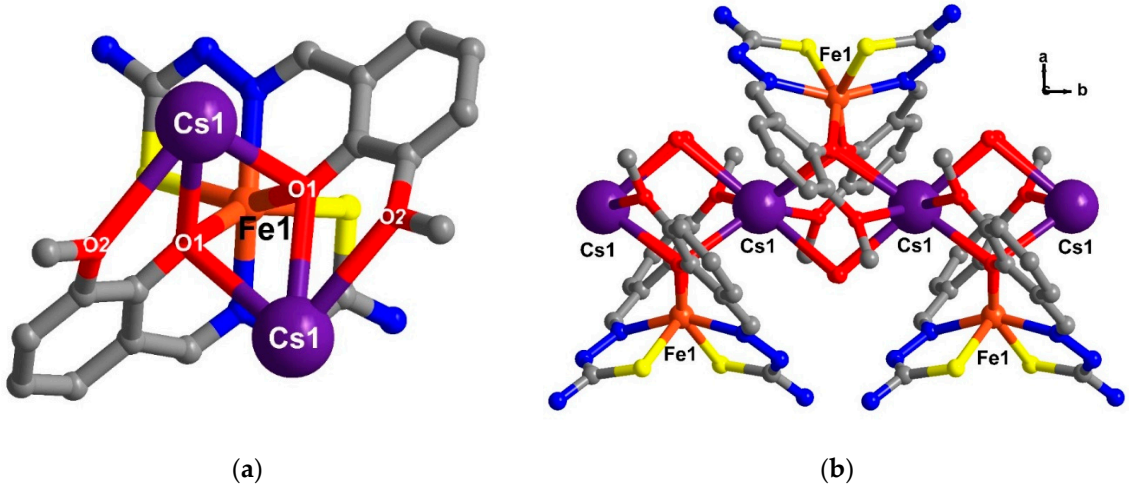

(**a**) (**b**)

Figure 7. Representation of (**a**) the coordination bonds between Cs cations and adjacent Fe(III) molecules and (**b**) a 1D chain polymeric motif in **5**.

For homoleptic Fe(III)-thsa compounds containing Cs cations, in addition to **5** and **6,** there are $Cs[Fe(thsa)_2]$ [10] and $Cs[Fe(5\text{-}Br\text{-}thsa)_2]$ [11] that have been reported to show HS and LS behaviour, respectively, at 293 K. It is interesting to note that the Cs cation always form a Cs–O bond with the oxygen that directly bonds to the Fe(III) centre and this can be expected to affect the electronic structure. Unfortunately, in **5** and **6** it gives rise to an inappropriate ligand field energy gap for SCO to take place and, subsequently, leads to invariant HS or LS behaviour in these Fe(III)-thsa-Cs systems within the experimental ranges measured. Interestingly, in the related Fe(III)-thsa compound, $K[Fe(5\text{-}Br\text{-}thsa)_2]$ [12] that has a similar structure to $Cs[Fe(5\text{-}Br\text{-}thsa)_2]$ [11], the compound was reported to show SCO with thermal hysteresis above 350 K (for $T_{1/2}\uparrow$ = 358 K) [12]. Thus, the s-block cation plays a role but one that is hard to predict.

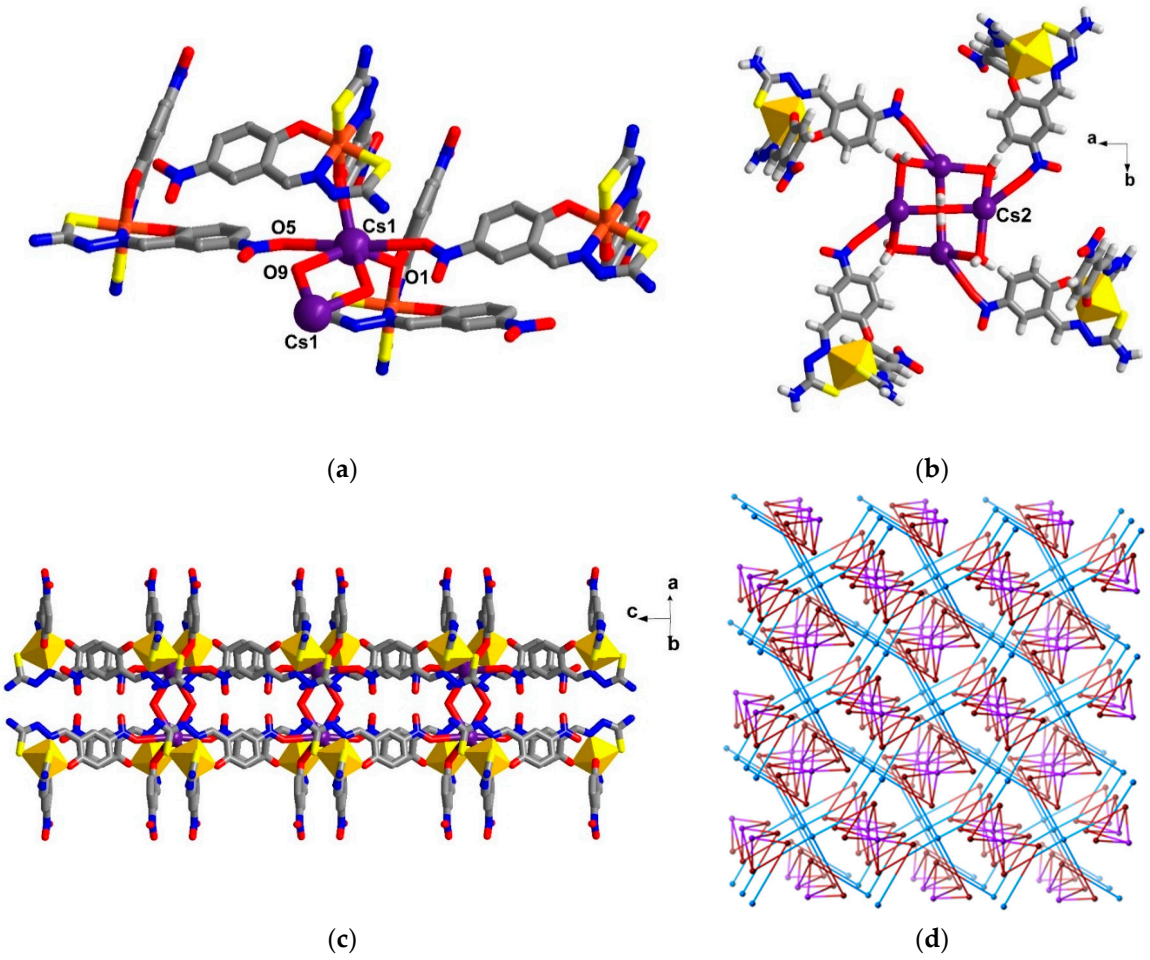

Figure 8. Representations of **6** show (**a**) the coordinating atoms surrounding Cs1 (**b**) the cluster of Cs2 cations, (**c**) a 1D polymer of [Fe(5-NO_2-thsa)$_2$] and Cs1 with water bridges and (**d**) the underlying 3,4,8-c 3D network with $(4.8^2)_4(8^6)(4^{12}.8^8.10^8)$ topology (brown spheres represent [Fe(5-NO_2-thsa)$_2$] moieties, blue spheres represent Cs_4 clusters, and purple spheres represent Cs_2 clusters).

3. Materials and Methods

3.1. General

All reagents and solvents were purchased from Sigma–Aldrich Australia (Castle Hill, NSW, 1765, Australia) and used as received. Infrared spectra were measured with a Bruker Equinox 55 FTIR spectrometer fitted with a 71Judson MCT detector and Specac Golden Gate diamond ATR. Microanalyses were performed by Campbell Microanalytical Laboratory, Department of Chemistry, University of Otago, Dunedin, New Zealand. Variable-temperature magnetic susceptibility data were collected with either a Quantum Design MPMS 5 superconducting quantum interference device (SQUID) magnetometer or a MPMS XL-7 SQUID magnetometer, with a scan speed of 10 K·min^{-1} followed by a one-minute wait after each temperature change.

X-ray crystallographic measurements for compounds **2**, **3** and **4** were collected at the Australian Synchrotron operating at approximately 16 keV (λ = 0.71073 Å). Single crystals were mounted on a glass fibre using oil. The collection temperature, 100 K, was maintained at specified temperatures using an open-flow N_2 cryostream. Data were collected using Blue Ice software [13]. Initial data processing was carried out using the XDS package [14]. X-ray data for **1** have been published [5].

X-ray crystallographic measurements on **5** and **6** were collected at 123 K using a Bruker Smart Apex X8 diffractometer with Mo-$K\alpha$ radiation (λ = 0.71073 Å). Single crystals were mounted on a

glass fibre using oil. The data collection and integration were performed within SMART and SAINT+ software programs and corrected for absorption using the Bruker SADABS program [15]. For **6**, one of the Cs atoms (Cs2) was refined at half occupancy; higher occupancies led to unreasonably high anisotropic displacement parameters. Cambridge Crystallographic Data Base CCDC numbers are 1552514–1552518 for compounds **2**–**6**. The CCDC number for compound **1** is 1420398 [5].

X-ray powder diffraction patterns on **4** and **6**(**bulk**) were recorded using a Bruker D8 Advance powder diffractometer operating at Cu Kα wavelength (1.5418 Å), with samples mounted on a zero-background silicon single-crystal stage. Scans were performed at room temperature in the 2θ range 5°–55°.

3.2. Synthesis of Ligands

R-HSalEen, where R = 3-MeO and 3-EtO and R-H_2thsa, where R = 5-NO_2, 3-MeO and 3-EtO were synthesized according to the literature methods given in references [16,17], respectively.

3.3. Synthesis of Iron(III) Complexes

3.3.1. Synthesis of [Fe(3-MeOSalEen)(3-EtOthsa)] **2**

A solution of 3-MeO-HSalEen (0.4 mmol) in MeOH (3 mL) was on the top of the layered diffusion method in which NEt_3 (56 μL, 0.4 mmol) had been added as a base. The middle layer is the metal solution. $FeCl_3$ (36 mg, 0.2 mmol) was dissolved in n-BuOH (2 mL). The solution was stirred for 5 min and then layered onto the solution of 3-EtO-H_2thsa (50 mg, 0.2 mmol) in H_2O (3 mL), in which CsOH (72 mg, 0.4 mmol) had been added as a base. After 3 weeks, black hexagonal plate-crystals formed together with colourless plate-crystals of by-product salts. The crystals were filtered and dried under ambient conditions. After a day, the black crystals were separated manually under the microscope; yield 19 mg (18%). $\tilde{\upsilon}_{max}/cm^{-1}$ 3235 (υ_{NH2}), 3046 ($\upsilon_{Ar–H}$), 1595 ($\upsilon_{C=N}$), 1297 ($\upsilon_{C–O}$), 731 (υ_{CS}) cm^{-1}. *m*/*z* (ESI) 515.2 [Fe(3-MeOSalEen)(3-EtOthsa)]. Calcd. for [Fe(3-MeOSalEen)(3-EtOthsa)] (found %) $C_{22}H_{28}FeN_5O_4S$: C, 51.37 (51.25); H, 5.49 (5.59); N, 13.61 (13.48).

3.3.2. Synthesis of [Fe(3-EtOSalEen)$_2$]NO_3 **3**

$Fe(NO_3)_3{\cdot}9H_2O$ (51 mg, 0.2 mmol) was dissolved in MeOH (5 mL). The solution was stirred for 5 min and then layered onto a solution of 3-EtO-HSalEen (95 mg, 0.4 mmol) in CH_2Cl_2 (2 mL), which was in the bottom layer to which NEt_3 (56 μL, 0.4 mmol) had been added as a base. After 7 days, the homogenous black solution was allowed to slowly evaporate in air. After a few days, black crystals formed, which were washed with acetone (2 × 1 mL) and then air-dried; yield 22 mg (18%). $\tilde{\upsilon}_{max}/cm^{-1}$ 3170 (υ_{NH}), 2933 ($\upsilon_{Ar–H}$), 1596 ($\upsilon_{C=N}$), 1246 ($\upsilon_{C–N}$), 1217 ($\upsilon_{C–O}$) cm^{-1}. *m*/*z* (ESI) 526.2 [Fe(3-EtOSalEen)$_2$]$^+$. Calcd. for [Fe(3-EtOSalEen)$_2$]$NO_3{\cdot}$MeOH$\cdot$0.5H_2O (found %) $C_{27}H_{43}FeN_5O_{8.5}$: C, 51.51 (51.16); H, 6.88 (7.13); N, 11.12 (11.74).

3.3.3. Synthesis of [Fe(3-EtOSalEen)$_2$]Cl **4**

The same synthesis procedure for compound **3** was used to prepare compound **4** as well. $FeCl_3$ (34 mg, 0.2 mmol) has been used instead of $Fe(NO_3)_3{\cdot}9H_2O$; yield 26 mg (23%). $\tilde{\upsilon}_{max}/cm^{-1}$ 3055 (υ_{NH}), 2922 ($\upsilon_{Ar–H}$), 1596 ($\upsilon_{C=N}$), 1247 ($\upsilon_{C–N}$), 1218 ($\upsilon_{C–O}$) cm^{-1}. *m*/*z* (ESI) 526.3 [Fe(3-EtOSalEen)$_2$]$^+$. Calcd. for [Fe(3-EtO-SalEen)$_2$]Cl (found %) $C_{26}H_{38}ClFeN_4O_4$: C, 55.58 (57.16); H, 6.82 (7.50); N, 9.97 (9.35). This analysis is on the sample giving the PXRD in Figure S1.

3.3.4. Synthesis of CsH_2O[Fe(3-MeOthsa)$_2$] **5**

$FeCl_3$ (39 mg, 0.2 mmol) was dissolved in MeOH (3 mL). The solution was stirred for 5 min and then layered on the solution of 3-MeO-H_2thsa (92 mg, 0.4 mmol) in H_2O (2 mL), which was in the bottom, in which CsOH (134 mg, 0.8 mmol) had been added as a base. After 7 days, black crystals formed, these were washed with acetone (2 × 1 mL) and then air-dried; yield 73 mg (56%).

$\tilde{\upsilon}_{max}/cm^{-1}$ 3291 (υ_{NH2}), 2959 (υ_{Ar-H}), 1594 ($\upsilon_{C=N}$), 1237 (υ_{C-N}), 1215 (υ_{C-O}) 728 (υ_{C-S}) cm^{-1}. *m*/*z* (ESI) 501.9 $[Fe(3\text{-}MeOthsa)_2]^-$. Calcd. for $CsH_2O[Fe(3\text{-}MeOthsa)_2]$ (found %) $C_{18}H_{20}CsFeN_6O_5S_2$: C, 33.09 (33.27); H, 3.08 (2.94); N, 12.86 (12.75).

3.3.5. Synthesis of $Cs(H_2O)_2[Fe(5\text{-}NO_2\text{-}thsa)_2]$ **6**(**bulk**)

$FeCl_3$ (39 mg, 0.2 mmol) was dissolved in MeOH (3 mL). The solution was stirred for 5 min and then layered on the solution of 5-NO_2-H_2thsa (97 mg, 0.4 mmol) in H_2O (3 mL), which was in the bottom, in which CsOH (146 mg, 0.8 mmol) had been added as a base. After 7 days, black crystals formed, which were washed with acetone (2 × 1 mL) and then air-dried; yield 34 mg (24%). $\tilde{\upsilon}_{max}/cm^{-1}$ 3255 (υ_{NH2}), 3013 (υ_{Ar-H}), 1587 ($\upsilon_{C=N}$), 1277 (υ_{C-N}) 737 (υ_{C-S}) cm^{-1}. *m*/*z* (ESI) 532.0 $[Fe(5\text{-}NO_2\text{-}thsa)_2]^-$. Calcd. for $Cs(H_2O)_2$ $[Fe(5\text{-}NO_2\text{-}thsa)_2]$.CsOH (found %) $C_{16}H_{17}Cs_2FeN_8O_9S_2$: C, 22.50 (22.73); H, 1.90 (1.90); N, 13.18 (11.87). This analysis is on the sample giving the PXRD in Figure S1.

4. Conclusions

Three groups of Fe(III) compounds with various tridentate Schiff base ligands, i.e., heteroleptic: [Fe(3-OMeSalEen)(thsa)] **1** and [Fe(3-MeOSalEen)(3-EtOthsa)] **2**, cationic homoleptic: $[Fe(3\text{-}EtOSal\ Een)_2]NO_3$ **3** and $[Fe(3\text{-}EtOSalEen)_2]Cl$ **4** and anionic homoleptic: $CsH_2O[Fe(3\text{-}MeOthsa)_2]$ **5** and $Cs(H_2O)_2[Fe(5\text{-}NO_2\text{-}thsa)_2]$ **6** have been investigated. Complexes **2**–**6** were newly synthesized and studied for the first time. Magnetic studies of the compounds revealed incomplete SCO for **2**–**4**, while **5** and **6**(**bulk**) showed HS and LS behaviour up to 360 K, respectively. It is interesting to note that the spin transition in **2**–**4** starts to take place at high temperature especially in the cases of **3** and **4**, above 340 K.

In comparison among each group, for **1** and **2**, an ethoxy substitution on the $thsa^{2-}$ ligand results in less order of the molecular packing and, thus, a lower ability to form a potential intermolecular interaction. Consequently, it has poorer cooperativity than the analogous unsubstituted compound **1**, thus exhibiting more gradual and incomplete SCO up to 360 K. In the case of the homoleptic cationic compounds **3** and **4**, which are isostructural, stronger hydrogen bonds between the anions and the Fe(III) moieties are suggested to be responsible for an abrupt spin change observed in **3**, at 343 K, accompanied by hysteresis, which compares to a small, gradual SCO change in **4**. The anionic homoleptic compounds **5** and **6** are somewhat distinct in behaviour. With a preference for their co-cation Cs to form a bond with oxygen atoms, the resulting Cs–O bonds link the Fe(III) molecules into a coordination polymer forming a 1D chain for **5** and a 3D network for **6**. However, direct bonding of Cs^+ to an oxygen donor yields the inappropriate ligand field around the Fe(III) centres in **5** and **6**. Consequently, there is no spin transition taking place in the experimental temperature region for these two compounds.

Supplementary Materials: The following are available online at www.mdpi.com/2304-6740/5/3/51/s1, Tables S1–S7, structural details. Figure S1, Powder X-ray diffractograms, observed and simulated, for **4** and **6**(**bulk**). Figure S2, plots of magnetic data for **2** to **6**. Figures S3–S12, structural details and comparisons. CIF files and checkcif reports.

Acknowledgments: This work was supported by an Australian Research Council Discovery grant (to KSM). Access to the Australian Synchrotron is gratefully acknowledged. Boujemaa Moubaraki, Monash University, is thanked for help with magnetic studies.

Author Contributions: Luke Darveniza and Wasinee Phonsri synthesized and characterized all compounds, Keith Murray and Wasinee Phonsri planned the research. Wasinee Phonsri collected the X-ray data, refined the crystal structures, with Stuart Batten's involvement, and measured the magnetic properties. Wasinee Phonsri wrote the first draft, Keith Murray and Stuart Batten proofread and prepared the final version of the manuscript.

Conflicts of Interest: The authors declare no conflict of interest.

References

1. Murray, K.S. The development of spin-crossover research. In *Spin-Crossover Materials: Properties and Applications*; Halcrow, M.A., Ed.; John Wiley & Sons Ltd.: Chichester, UK, 2013; pp. 1–54.
2. Gütlich, P.; Goodwin, H.A. *Spin Crossover in Transition Metal Compounds I–III*; Springer: Berlin/Heidelberg, Germany, 2004; pp. 232–235.
3. Harding, D.J.; Harding, P.; Phonsri, W. Spin crossover in iron(III) complexes. *Coord. Chem. Rev.* **2016**, *313*, 38–61. [CrossRef]
4. Kennedy, B.J.; McGrath, A.C.; Murray, K.S.; Skelton, B.W.; White, A.H. Variable-temperature magnetic, spectral, and X-ray crystallographic studies of "spin-crossover" iron(III) schiff-base-lewis-base adducts. Influence of noncoordinated anions on spin-state interconversion dynamics in [Fe(salen)$(imd)_2$]Y species (Y = ClO_4^-, BF_4^-, PF_6^-, BPh_4^-; imd = imidazole). *Inorg. Chem.* **1987**, *26*, 483–495.
5. Phonsri, W.; Martinez, V.; Davies, C.G.; Jameson, G.N.L.; Moubaraki, B.; Murray, K.S. Ligand effects in a heteroleptic bis-tridentate iron(III) spin crossover complex showing a very high $T_{1/2}$ value. *Chem. Commun.* **2016**, *52*, 1443–1446. [CrossRef] [PubMed]
6. McCusker, J.K.; Rheingold, A.L.; Hendrickson, D.N. Variable-temperature studies of laser-initiated $^5T_2 \rightarrow {}^1A_1$ intersystem crossing in spin-crossover complexes: Empirical correlations between activation parameters and ligand structure in a series of polypyridyl ferrous complexes. *Inorg. Chem.* **1996**, *35*, 2100–2112. [CrossRef]
7. Marchivie, M.; Guionneau, P.; Letard, J.-F.; Chasseau, D. Photo-induced spin-transition: The role of the iron(II) environment distortion. *Acta Crystallogr. Sect. B Struct. Sci.* **2005**, *61*, 25–28. [CrossRef] [PubMed]
8. Russell, V.; Scudder, M.; Dance, I. The crystal supramolecularity of metal phenanthroline complexes. *J. Chem. Soc. Dalton Trans.* **2001**, *6*, 789–799. [CrossRef]
9. Steiner, T. The hydrogen bond in the solid state. *Angew. Chem. Int. Ed.* **2002**, *41*, 48–76. [CrossRef]
10. Ryabova, N.A.; Ponomarev, V.I.; Zelentsov, V.V.; Atovmyan, L.O. Kristallografiya. *Russ. Crystallogr. Rep.* **1981**, *26*, 101.
11. Powell, R.E.; Schwalbe, C.H.; Tizzard, G.J.; Koningsbruggen, P.J.V. Caesium bis(5-bromosalicylaldehyde thiosemicarbazonato-κ^3 O,N,S)ferrate(III): Supramolecular arrangement of low-spin Fe^{III} complex anions mediated by Cs^+ cations. *Acta Cryst.* **2015**, *C71*, 169–174.
12. Kang, S.; Shiota, Y.; Kariyazaki, A.; Kanegawa, S.; Yoshizawa, K.; Sato, O. Heterometallic Fe^{III}/K coordination polymer with a wide thermal hysteretic spin transition at room temperature. *Chem. Eur. J.* **2016**, *22*, 532–538. [CrossRef] [PubMed]
13. McPhillips, T.M.; McPhillips, S.E.; Chiu, H.-J.; Cohen, A.E.; Deacon, A.M.; Ellis, P.J.; Garman, E.; Gonzalez, A.; Sauter, N.K.; Phizackerley, R.P.; et al. Blu-ice and the distributed control system: Software for data acquisition and instrument control at macromolecular crystallography beamlines. *J. Synchrotron Radiat.* **2002**, *9*, 401–406. [CrossRef] [PubMed]
14. Kabsch, W. Automatic processing of rotation diffraction data from crystals of initially unknown symmetry and cell constants. *J. Appl. Crystallogr.* **1993**, *26*, 795–800. [CrossRef]
15. Sheldrick, G.M. *SADABS, Program for Area Detector Adsorption Correction*; Institute for Inorganic Chemistry, University of Göttingen: Göttingen, Germany, 1996.
16. Hui, R.-H.; Zhou, P.; You, Z.-L. Syntheses and crystal structures of two azide-bridged dinuclear zinc(II) complexes with schiff bases and halides. *Synth. React. Inorg. Met. Org. Nano Met. Chem.* **2012**, *42*, 135–139. [CrossRef]
17. Mehta, B.H.; Shaikh, J.A. Synthesis, characterisation, X-ray diffraction and antimicrobial studies of Pd(II), Rh(III) and Ru(III) complexes of thiosemicarbazones. *J. Ind. Counc. Chem.* **2009**, *26*, 1–6.

© 2017 by the authors. Licensee MDPI, Basel, Switzerland. This article is an open access article distributed under the terms and conditions of the Creative Commons Attribution (CC BY) license (http://creativecommons.org/licenses/by/4.0/).